Water and Wastewater, Vol. 35, No. 6, pp: 20-25

Facile Synthesis of g-C_3N_{4-x} for the Effective Destruction/Removal of Organic Pollutants from Water and Wastewater

Hosna Rezaei[1], Hani Sayahi[2*]

1. PhD. Researcher at Dept. of Physical Chemistry, Chemical Process Development Institute, Chemistry and Chemical Engineering Research Center of Iran (CCERCI), Tehran, Iran, P. O. Box. 14335-186
2. Assoc. Prof. of Physical Chemistry, Dept. of Physical Chemistry, Chemical Process Development Institute, Chemistry and Chemical Engineering Research Center of Iran (CCERCI), Tehran, Iran, P. O. Box. 14335-186 (Corresponding Author) sayahi@ccerci.ac.ir

https://doi.org/10.22093/wwj.2025.515357.3482 **Original Paper**

Abstract

In response to the urgent global issue of environmental pollution, particularly water contamination by high-chroma organic pollutants, there has been a growing focus within the scientific community on developing advanced materials for efficient pollutant removal. One such promising material is graphene-like carbon nitride (g-C_3N_4), which possesses excellent chemical stability, high surface area, and photocatalytic properties. This essay delves into the facile synthesis of g-C_3N_{4-x} for effectively removing high-chroma organic pollutants from water, exploring its potential applications, advantages, and prospects. Additionally, a g-C_3N_{4-x} photocatalyst has been synthesized in this study by introducing nitrogen vacancies through a one-step reduction process. The optimized g-C_3N_{4-x} catalyst exhibited a superior MB and TC yield of 73% and 83.6%, respectively, under visible light, representing a 4.5-fold increase compared to the bulk g-C_3N_4 catalyst. This advancement is attributed to the synergistic effects of nitrogen vacancies defects, which enhance light absorption, facilitate electron-hole pair separation, and increase the number of active sites on the catalyst surface. In our research, we successfully created a g-C_3N_{4-x} photocatalyst by incorporating nitrogen vacancies using a one-step reduction technique. The optimized g-C_3N_{4-x} catalyst displayed an impressive 73% MB and 83.6% yield for TC under visible light, 4.5 times higher than the standard g-C_3N_4 catalyst. This improvement is attributed to the synergistic effects of nitrogen vacancies defects, which enhance light absorption, aid in separating electron-hole pairs, and increase the number of active sites on the catalyst's surface.

Keywords:
Renewable Energy, Photocatalyst, Graphite Carbon Nitride, Environmental Organic Pollutants.

Received: Jan. 3, 2025
Revised: Jan. 29, 2025
Accepted: Feb. 9, 2025

To cite this article:
Rezaei, H., Sayahi, H., 2025. Facile synthesis of g-C_3N_{4-x} for the effective destruction/removal of organic pollutants from water and wastewater. *Water and Wastewater*, 35(6), 20-25. https://doi.org/10.22093/wwj.2025.515357.3482.

Use your device to scan and read the article online

1. Introduction

In recent years, environmental pollution has become a pressing global issue, with water contamination by high-chroma organic pollutants posing a significant threat to human health and ecosystem integrity. As a response to this challenge, the development of advanced materials for efficient removal of such pollutants has gained increasing attention in the scientific community (Wang et al., 2018a; Wang et al., 2018b).

Traditional methods to remove organic pollutants from water include adsorption, ultrafiltration, reverse osmosis, chemical coagulation, and biodegradation. While effective, these methods are often costly and difficult to reuse on a large scale. A better solution is the Advanced Oxidation Process[1] using photocatalysis, which uses light to break down harmful chemicals. This method, especially with semiconductor materials, shows promise for degrading contaminants using solar energy. One promising candidate semiconductor is graphene-like carbon nitride (g-C_3N_4), with excellent chemical stability, high surface area, and photocatalytic properties (Dong et al., 2014).

Although g-C_3N_4 has advantages, it suffers from a limited surface area and poor separation efficiency. To further enhance the photocatalytic activity, the synthesis of g-C_3N_{4-x} involves a straightforward and cost-effective approach that allows for rapid adsorption of pollutants onto its surface, enhancing the overall removal efficiency. Typically, g-C_3N_{4-x} can be synthesized by thermally treating precursors such as melamine at elevated temperatures in the presence of a suitable catalyst or template. This process yields a porous structure with a high surface area, facilitating the adsorption of organic pollutants and promoting their degradation through photocatalytic reactions (Niu et al., 2012).

One of the key advantages of g-C_3N_{4-x} is its efficient removal of high-chroma organic pollutants from water. The unique structural and electronic properties of g-C_3N_{4-x} enable it to generate reactive oxygen species under light irradiation, which can effectively oxidize and degrade a wide range of organic pollutants, including dyes, pesticides, and pharmaceuticals. Moreover, the high surface area of g-C_3N_{4-x} allows for rapid adsorption of pollutants onto its surface, enhancing the overall removal efficiency. In addition to its high removal efficiency, g-C_3N_{4-x} exhibits excellent stability and reusability, making it a sustainable and cost-effective solution for water treatment. Unlike traditional adsorbents or photocatalysts, g-C_3N_{4-x} can be easily regenerated by simple washing or thermal treatment, allowing for multiple cycles of pollutant removal without significant loss of performance. This reduces the operational costs of water treatment and minimizes the environmental impact of the disposal of used materials. Furthermore, the simple synthesis of g-C_3N_{4-x} opens up new possibilities for designing and engineering advanced materials with tailored properties for specific pollutant removal applications. By adjusting the synthetic conditions, such as precursor composition, temperature, and duration of thermal treatment, researchers can fine-tune the structure and morphology of g-C_3N_{4-x} to enhance its photocatalytic activity, adsorption capacity, and selectivity towards target pollutants (Feng et al., 2020; Antonietti and Fratzl, 2010).

This level of control over material properties allows for customized solutions for different water treatment scenarios, from industrial wastewater remediation to municipal water purification. In conclusion, the simple synthesis of g-C_3N_{4-x} offers great potential for efficiently removing high-chroma organic pollutants from water, providing a sustainable and cost-effective solution to the pressing environmental challenge of water contamination. By harnessing the unique properties of g-C_3N_{4-x}, researchers can develop innovative materials with enhanced performance and versatility for various pollutant removal applications. With continued research and development in this field, g-C_3N_{4-x} is poised to make a significant impact on water treatment technologies, paving the way toward a cleaner and healthier environment for future generations (Lotsch et al., 2007; Ouyang et al., 2020).

2. Experimental detail

2.1. Catalyst synthesis

2.1.1. Preparation of g-C_3N_4

The g-C_3N_4 nanosheets were prepared by Melamine calcination. This involved pouring 10 g of Melamine into a crucible and then heating it in a muffle furnace. The temperature was increased to 300 °C at a rate of 15 °C per minute, and then further increased to 550 °C for 4 hours to obtain a fine yellowish powder.

2.1.2. Preparation of g-C_3N_{4-x}

The N-deficient g-C_3N_4 was synthesized through the following procedure: 10 g of Melamine were thoroughly mixed with a specific quantity of NaOH and subsequently placed into a covered ceramic crucible. The mixture was then heated to 550 °C as same as g-C_3N_4. The resulting products were denoted g-C_3N_{4-x}(N). The preparation of pristine g-C_3N_4 followed the same procedural steps but omitted the addition of NaOH. Post-synthesis, all samples underwent extensive washing with deionized water and alcohol to eliminate any residual NaOH.

[1] Advanced Oxidation Process (AOP)

3. Result and discussion

3.1. Characterization

Fig. 1 shows the XRD patterns of pristine g-C_3N_4 and modified g-C_3N_{4-x}. The two materials exhibit a similar crystalline structure. The main diffraction peaks occur at around 13.0 and 27.3, representing the in-plane structural repeating motifs of aromatic systems and the interlayer reflection of the graphitic structure, respectively. When comparing g-C_3N_4 to g-C_3N_{4-x}, a slight shift in the latter peak is observed, from 27.15 to 27.35, indicating a decrease in the interlayer stacking distance from 3.28 nm to 3.24 nm. have also observed a similar shift when nitrogen defects were present in g-C_3N_{4-x}. This might be attributed to the removal of nitrogen-containing species from the g-C_3N_4 skeleton, leading to a decrease in interlayer repulsion and an increase in interlayer stacking density (Niu et al., 2012).

The FTIR spectra of g-C_3N_4 and g-C_3N_{4-x} were displayed in Fig. 2.

The strong peak at around 3200 cm^{-1} is caused by the stretching of N-H bonds. The characteristic peaks between 1200 and 1600 cm^{-1}, including bands at 1238, 1319, 1407, 1458 and 1541 cm^{-1}, correspond to the stretching vibration of C-N heterocycles. Additionally, the peak at 807 cm^{-1} is attributed to the vibrations of triazine units (Montigaud et al., 2000; Li et al., 2004).

Fig. 3 shows the FESEM images of two structures: a) pristine g-C_3N_4 and b) modified g-C_3N_{4-x}. Upon closer examination of the latter structure, it is evident that there has been a significant decrease in particle size and an increase in the number of pores, as well as the depth to which they extend.

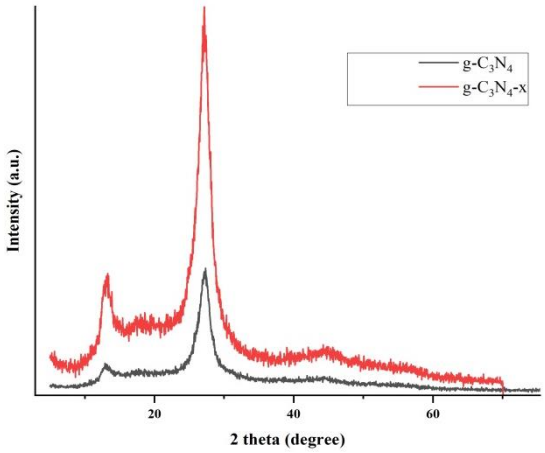

Fig. 1. The XRD spectra of g-C_3N_4 and g-C_3N_{4-x}

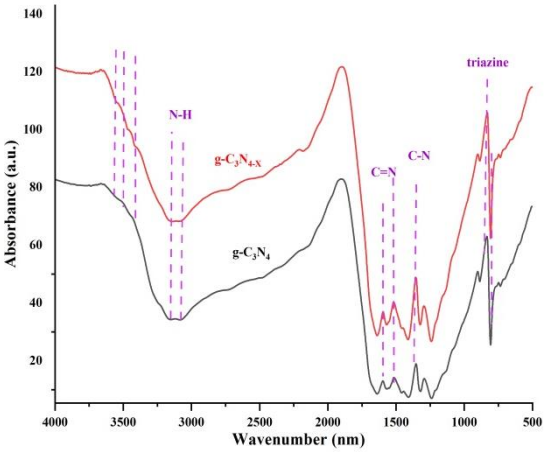

Fig. 2. The FTIR spectra of g-C_3N_4 and g-C_3N_{4-x}

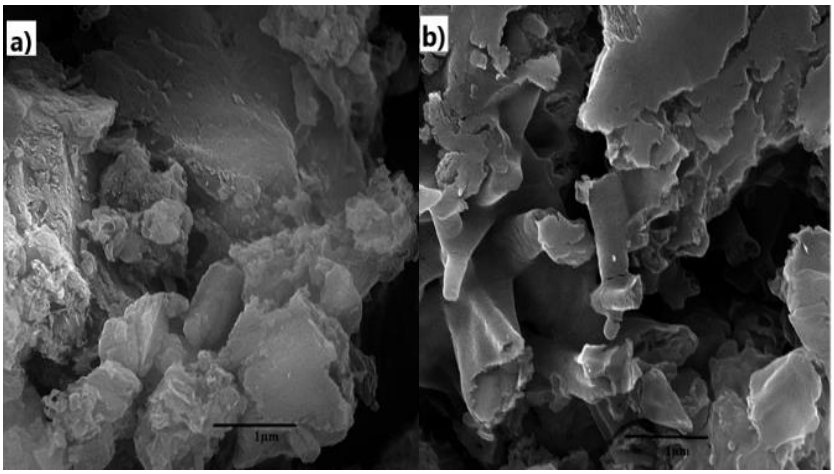

Fig. 3. Shows the FESEM of two structures of a) pristine g-C_3N_4 and b) modified g-C_3N_{4-x}

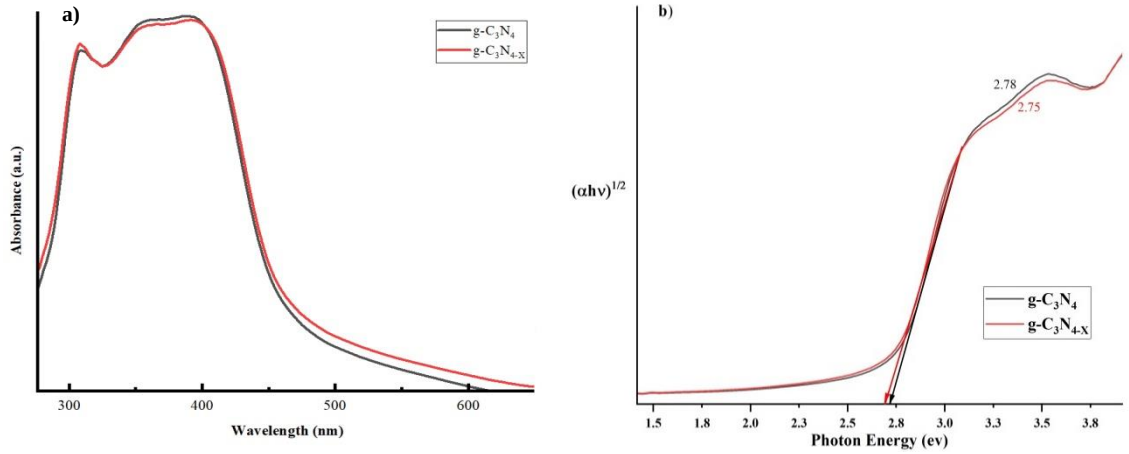

Fig. 4. a) Demonstrates the optical absorption properties of synthesized g-C_3N_4 and g-C_3N_{4-x} via UV-visible spectroscopy RT and b) presents the band gap values of g-C_3N_4 and g-C_3N_{4-x}

Fig. 4a) demonstrates the optical absorption properties of synthesized g-C_3N_4 and g-C_3N_{4-x} via UV-visible spectroscopy at room temperature[1], spanning 250-700 nm. The red line for g-C_3N_{4-x} shows a notable absorption peak at 460 nm. Fig. 4b) presents the band gap values of g-C_3N_4 and g-C_3N_{4-x}, determined by the Tauc plot, which are 2.78 eV and 2.75 eV, respectively, highlighting their potential in various applications (Arya et al., 2018).

The specific surface area of the g-C_3N_4 sample, calculated from N_2 isotherms, was found to be 6.11 m^2/g. Following modification, there are only slight differences in the N_2 isotherms and pore size distributions between g-C_3N_4 and g-C_3N_{4-x}. Notably, the BET surface areas of g-C_3N_{4-x} have improved, increasing to 12.3 ± 0.1 m^2/g, demonstrating the effectiveness of the modification process.

3.2. Photocatalytic activity

The wastewater from dyes is known for its high chroma and resistance to degradation, posing a significant threat to the environment. Typical dyes found in wastewater include MB, rhodamine B, and methyl orange, which contaminate water and can harm human health. In our experiment, MB is used as a model to assess the adsorption-photocatalysis performance of the samples. Fig. 5 presents the adsorption-photocatalysis removal of MB by g-C_3N_4 and g-C_3N_{4-x}. Before 0 minutes, the samples underwent dark adsorption, reaching adsorption-desorption equilibrium at 0 minutes, and then proceeded to the photocatalytic degradation of MB. This experiment was also done for TC, whose result is shown in Fig. 6a and 6b. As seen, g-C_3N_{4-x} demonstrated excellent adsorption performance (>73%) due to the large specific surface area and electronic properties of g-C_3N_{4-x}, enabling the generation of reactive oxygen species under light irradiation to effectively oxidize and degrade a wide range of MB and TC. Additionally, the high surface area of g-C_3N_{4-x} allows for rapid adsorption of contaminants onto its surface, enhancing the overall removal efficiency. Effective adsorption not only traps pollutants on the sample surface but also reduces the concentration and chromaticity of the wastewater, thereby facilitating the subsequent photocatalytic degradation of pollutants.

Under visible light irradiation, graphitic carbon nitride (g-C_3N_{4-x}) absorbs photons to generate electron–hole pairs, where the photogenerated electrons reduce molecular oxygen to form superoxide radicals (•O_2^-) and the holes oxidize water or hydroxide ions to produce hydroxyl radicals (•OH); these reactive oxygen species then attack and degrade tetracycline molecules through oxidative reactions, ultimately breaking them down into smaller, less toxic intermediates or mineralizing them into CO_2 and H_2O.

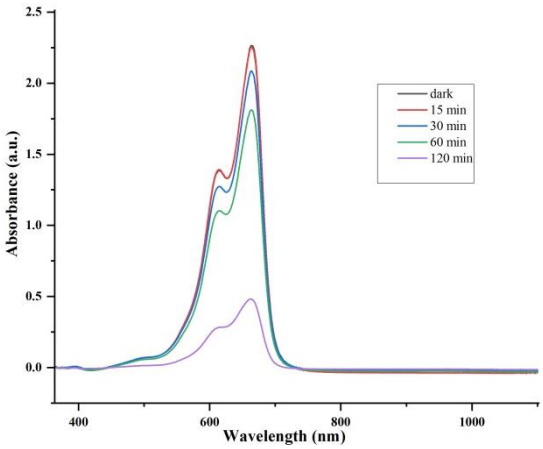

Fig. 5. In order a) adsorption-photocatalysis removal of high-chroma MB solution (25 ppm) by g-C_3N_{4-x}

[1] Room Temperature (RT)

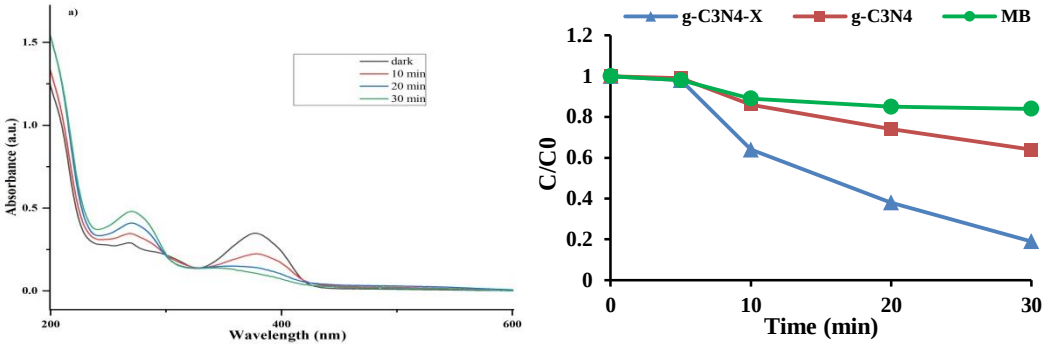

Fig. 6. a) Adsorption-photocatalysis removal of high-chroma TC solution (25 ppm) by g-C_3N_{4-x}. b) Photocatalytic degradation performance of g-C_3N_4 and g-C_3N_{4-X}

Summary Mechanism Diagram

1. Photon absorption → e^-/h^+ generation
2. Charge separation → Surface migration
3. ROS generation: $\bullet O_2^-$, •OH
4. TC degradation → Intermediates → Mineralization

Also, a reusability test was performed by MB. Fig. 7 shows the cycle of g-C_3N_{4-x} photocatalytic degradation, revealing a gradual decrease in degradation percentage from 84% in the first cycle to 75% in the fourth.

The absorbance changes of MB at 664 nm over time were recorded to assess the photocatalytic degradation kinetics of the organic pollutant. The data using pseudo-first-order and pseudo-second-order models were analyzed assuming that absorbance directly correlates with dye concentration. The pseudo-first-order kinetic model is expressed as follows

$$k_{1t} = \ln\left(\frac{a_0}{a_t}\right) \quad (1)$$

and the pseudo-second-order model as

$$k_{2t} = \frac{1}{A_0} - \frac{1}{A_t} \quad (2)$$

Table 1. Results of the photocatalytic degradation kinetics

Kinetic model	Pollutant	R^2	RMSE	Rate constant (k)
Pseudo-first-order	Dye	0.9875	0.0574	0.05446 min^{-1}
Pseudo-first-order	Tetracycline	0.9948	0.0348	0.06496 min^{-1}
Pseudo-second-order	Dye	0.9839	0.3121	0.22255 (1/A)/min
Pseudo-second-order	Tetracycline	0.9863	0.2482	0.28517 (1/A)/min

The results of the photocatalytic degradation kinetics for MB and TC are presented in Table 1.

These results indicate that the photocatalytic degradation follows a pseudo-first-order kinetic behavior, suggesting that a single molecular process or surface reaction likely governs the rate-limiting step.

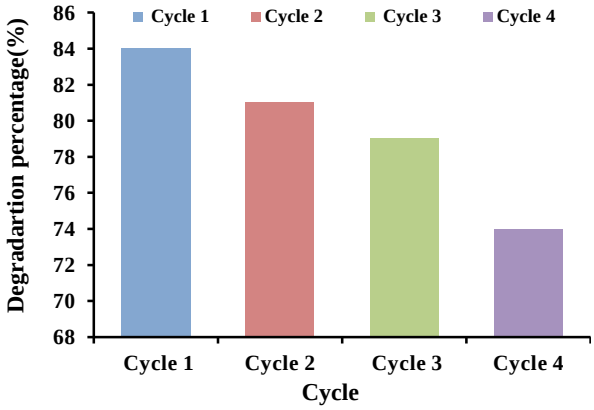

Fig. 7. Cycle of g-C_3N_{4-x} photocatalytic degradation

4. Conclusions

In summary, nitrogen defects were introduced into g-C_3N_4 through a hydrothermal method that utilized sodium hydroxide as an oxidizing agent. The resulting nitrogen-deficient g-C_3N_4 catalyst retains a crystalline phase composition and specific surface area that closely resembles those of pristine g-C_3N_4. However, this modified catalyst notably improves visible-light absorption and charge separation efficiency.

Incorporating nitrogen defects significantly enhances the photocatalytic degradation rate of pollutants, reaching an impressive rate of 83.6, approximately four times greater than that of the original g-C_3N_4 catalyst. Furthermore, the deficiency of amino species within the g-C_3N_4 framework benefits its overall properties. The newly introduced interband levels resulting from these

nitrogen defects are crucial for the observed improvements in photocatalytic performance, allowing the catalyst to excel in various applications involving pollutant degradation. The nitrogen-deficient g-C_3N_4 catalyst has a crystalline phase composition and specific surface area similar to that of pristine g-C_3N_4, but it shows improved visible-light absorption and charge separation efficiency. The introduction of nitrogen defects leads to a stable increase in the photocatalytic pollutant degradation rate, reaching up to 73.6 for MB and 83.6 for TC, about 4 times higher than that of g-C_3N_4. Also the reusability test evealing 75% photocatalytic degradation of MB after four cycles. The deficiency of amino species on g-C_3N_4 is found to have a positive impact on its properties, and the newly induced interband levels are responsible for the enhanced photocatalytic performance.

5. Acknowledgements

The authors would like to express their sincere gratitude to by the Chemistry & Chemical Engineering Research Center of Iran[1] for providing the necessary research facilities and support. We also gratefully acknowledge the financial support from CCERCI, which made this work possible.

[1] Chemistry & Chemical Engineering Research Center of Iran (CCERCI)

References

Antonietti, M. and Fratzl, P., 2010. Biomimetic principles in polymer and material science. *Macromolecular Chemistry and Physics*, 211, 166-170. https://doi.org/10.1002/macp.200900515.

Arya, S., Riyas, M., Sharma, A., Singh, B., Prerna, Bandhoria, P., Khan, S., et al. 2018. Electrochemical detection of ammonia solution using tin oxide nanoparticles synthesized via sol-gel route. *Applied Physics A, Materials Science and Processing*, 124, 538. https://doi.org/10.1007/s00339-018-1968-8.

Dong, G., Zhang, Y., Pan, Q. and Qiu, J., 2014. A fantastic graphitic carbon nitride (g-C_3N_4) material: electronic structure, photocatalytic and photoelectronic properties. *Journal of Photochemistry and Photobiology C: Photochemistry Reviews*, 20, 33-50. https://doi.org/10.1016/j.jphotochemrev.2014.04.002.

Feng, C., Tang, L., Deng, Y., Wang, J., Luo, J., Liu, Y., et al. 2020. Synthesis of leaf-vein-like g-C_3N_4 with tunable band structures and charge transfer properties for selective photocatalytic H_2O_2 evolution. *Advanced Functional Materials*, 30, 2001922. https://doi.org/10.1002/adfm.202001922.

Li, C., Cao, C. B. and Zhu, H. S., 2004. Graphitic carbon nitride thin films deposited by electrodeposition. *Materials Letters*, 58, 1903-1906. https://doi.org/10.1016/j.matlet.2003.11.024.

Lotsch, B. V., Döblinger, M., Sehnert, J., Seyfarth, L., Senker, J., Oeckler, O., et al. 2007. Unmasking melon by a complementary approach employing electron diffraction, solid-state NMR spectroscopy and theoretical calculations-structural characterization of a carbon nitride polymer. *Chemistry-A European Journal*, 13, 4969-4980. https://doi.org/10.1002/chem.200601759.

Montigaud, H., Tanguy, B., Demazeau, G., Alves, I. and Courjault, S., 2000. C_3N_4: dream or reality? solvothermal synthesis as macroscopic samples of the C_3N_4 graphitic form. *Journal of Materials Science*, 35, 2547-2552. https://doi.org/10.1023/A:1004798509417.

Niu, P., Liu, G. and Cheng, H. M., 2012. Nitrogen vacancy-promoted photocatalytic activity of graphitic carbon nitride. *The Journal of Physical Chemistry C*, 116, 11013-11018. https://doi.org/10.1021/jp301026y.

Ouyang, X., Tang, L., Feng, C., Peng, B., Liu, Y., Ren, X., et al. 2020. Au/CeO_2/g-C_3N_4 heterostructures: designing a self-powered aptasensor for ultrasensitive detection of Microcystin-LR by density functional theory. *Biosensors and Bioelectronics*, 164, 112328. https://doi.org/10.1016/j.bios.2020.112328.

Wang, H., Jiang, S., Shao, W., Zhang, X., Chen, S., Sun, X., et al. 2018a. Optically switchable photocatalysis in ultrathin black phosphorus nanosheets. *Journal of the American Chemical Society*, 140, 3474-3480. https://doi.org/10.1021/jacs.8b00719.

Wang, J., Tang, L., Zeng, G., Deng, Y., Dong, H., Liu, Y., et al. 2018b. 0D/2D interface engineering of carbon quantum dots modified Bi_2WO_6 ultrathin nanosheets with enhanced photoactivity for full spectrum light utilization and mechanism insight. *Applied Catalysis B: Environmental*, 222, 115-123. https://doi.org/10.1016/j.apcatb.2017.10.014.